Biofuel blending reduces aircraft engine particle emissions at cruise conditions

Richard H. Moore,[1*] Kenneth L. Thornhill,[1,2] Bernadett Weinzierl,[3,4]
Daniel Sauer,[3,4], Eugenio D'Ascoli,[3,4] Brian Beaton,[1]
Andreas J. Beyersdorf,[1] Dan Bulzan,[6] Chelsea Corr,[1,5]
Ewan Crosbie,[1,5] Robert Martin,[1] Dean Riddick,[1]
Michael Shook,[1,2] Gregory Slover,[1] Christiane Voigt,[3]
Robert White,[1] Edward Winstead,[1,2] Richard Yasky,[1]
Luke D. Ziemba,[1] Anthony Brown,[7] Hans Schlager,[3]
and Bruce E. Anderson[1]

[1]NASA Langley Research Center, Hampton, VA, USA
[2]Science Systems and Applications, Hampton, VA, USA
[3]Deutsches Zentrum für Luft- und Raumfahrt (DLR), Oberpfaffenhofen, Germany
[4]Ludwig Maximillians University, Munich, Germany
[5]NASA Postdoctoral Program, Oak Ridge, TN, USA
[6]NASA Glenn Research Center, Cleveland, OH, USA
[7]National Research Council – Canada, XXX, Canada

[*]To whom correspondence should be addressed;
E-mail: richard.h.moore@nasa.gov.

Aviation aerosol emissions have a disproportionately large climatic impact because they are emitted high in the relatively pristine upper troposphere where they can form linear contrails and influence cirrus clouds. Research aircraft from NASA, DLR, and NRC Canada made airborne measurements of gaseous and aerosol composition and contrail microphysical properties be-

hind the NASA DC-8 aircraft at cruise altitudes. The DC-8 CFM-56-2C engines burned traditional medium-sulfur Jet A fuel as well as a low-sulfur Jet A fuel and a 50:50 biofuel blend. Substantial, two-to-three-fold emissions reductions are found for both particle number and mass emissions across the range of cruise thrust operating conditions. These observations provide direct and compelling evidence for the beneficial impacts of biojet fuel blending under real-world conditions.

The global aviation sector alone contributes 3.5-4.9% of the current anthropogenic radiative forcing due to emissions of fossil fuel CO_2 as well as aerosol particles that can alter the extent and properties of cirrus clouds (*1–5*). Of these impacts, the largest uncertainties are associated with aviation-induced cloudiness both directly from linear, persistent contrails and indirectly from the contribution of black carbon, organic, and sulfate aerosols that may act as cloud condensation nuclei (CCN) and ice nuclei (IN) (*6–9*). As fuel emissions of CO_2 are expected to more than double by 2050, the future aviation forcing may increase 3-4-fold over year 2000 levels (*1*), or even greater when using newer methods for estimating the direct radiative impact of engine-derived black carbon emissions (*10*). National and international regulatory and advisory bodies are exploring ways to curb these emissions, including coverage of aircraft flights originating or ending in EU airspace under the EU Emissions Trading Scheme since 2012 and the recent Advance Notice of Proposed Rulemaking by the US EPA to regulate aviation CO_2 emissions under the Clean Air Act (*11–13*). The International Air Transport Association (IATA) and Advisory Council for Aviation Research and Innovation in Europe (ACARE) have targeted carbon-neutral growth by 2020 and a 50-75% reduction in carbon emissions by 2050 (*14, 15*).

Sustainable biojet fuels are a promising route for mitigating greenhouse gas emissions and are a current investment focus in both the United States and European Union. The European Advanced Biofuels Flightpath aims to enable 2 million tons of sustainable aviation biofuels to

be use by 2020. Meanwhile, the U.S. Farm-to-fly initiative targets annual production of 1 billion gallons of drop-in renewable jet fuel by 2018. However, many challenges remain before aviation biofuels are widely adopted, particularly with regard to cost and sustainability. Jet fuels are more heavily-refined than the biofuels employed for surface transportation with the latter perhaps presenting a "better biomass opportunity cost", but also a myriad of alternative energy solutions other than liquid hydrocarbon-based fuels (*16, 17*). Biojet fuels consist of a mixture of C_9-C_{16} hydrocarbons that are formed via a two-step process. First, transesterification of plant and animal oils produces oxygenated, functionalized hydrocarbons whose low density and energy content and high freezing point make them not directly viable for aviation. Consequently, in a second step, these compounds are hydroprocessed to produce a hydrotreated ester and fatty acids (HEFA) fuel that possesses many of the properties of petroleum-derived jet fuels (***?****, 18*). Promising plant-based feed stocks for future aviation biofuels include Jatropha, Camelina, and algae (*?*).

Biojet fuels promise a future aviation fuel source that is not dependent on fossilized carbon, and also possess near-zero levels of sulfur and aromatic species that are common in petroleum-based jet fuels. Previous laboratory and ground test experiments using bio-based fuels or synthetic Fischer-Tropsch fuels produced from natural gas and coal feed stocks show the absence of fuel sulfur and aromatic species significantly reduces the black carbon and sulfate particle emissions from turboprop and turbofan engines (*19–22*). These results are important for quantifying the impact of aviation on local air quality near airports and hint that similar reductions are likely to hold for high-altitude cruise conditions; however, the engine operating conditions on the ground (e.g., temperature, pressure, fuel flow rates, fuel/air ratio, maximum thrust) are very different than those in flight. Unless we can quantify the emissions impacts associated with these low-sulfur and low-aromatic fuels under realistic flight conditions, it will be impossible for society to understand the role biojet fuels may play in the future of aviation.

NASA, DLR – The German Aerospace Agency, and National Research Council (NRC) Canada research aircraft carried out a series of flight experiments in Spring of 2013 and 2014 to quantify the real-world impacts of biofuel blending on jet engine emissions. Flights were conducted out of the NASA Armstrong Flight Research Center (AFRC) in Palmdale, CA, with the NASA DC-8 as the source aircraft. The DC-8 has four, wing-mounted CFM56-2-C1 engines that can be fed fuel from any of four segregated fuels tanks within the wings containing either a medium- or low-sulfur Jet A fuel as well as a fuselage-mounted auxiliary tank containing a 50:50 (v/v) blend of low-sulfur Jet A fuel and a Camelina-based HEFA biojet fuel. The medium-sulfur Jet A fuel was created by doping the the low-sulfur Jet A delivered from the refinery with a small aliquot of tetrahydrothiophene in order to increase the fuel sulfur content without changing the other fuel properties. The major difference between the HEFA fuel and traditional petroleum-based fuels is that the former possess no sulfur or aromatic species, while traditional jet fuels have aromatic contents near 18-25%. In addition to strict standards related to fuel density, viscosity, and freezing behavior that impact safety of flight, fuel aromatics are limited to below 25% in order to limit solvent deterioration of nitrile elastomers; meanwhile, a minimum aromatic content of 8% was established in order to swell the elastomer seals in the some current fuel systems (*23–25*). For this reason, only 50:50 blends of HEFA and petroleum-based fuels are currently certified for flight. All investigated fuels conform to flight worthiness specifications outlined by ASTM (*26, 27*), and detailed ACCESS fuel properties are detailed in the Supporting Online Material (SOM).

The left and right inboard DC-8 engine exhaust plumes (#2 and #3, respectively) were sampled by research aircraft flying in a trailing formation at a distance of 30-150 m behind the DC-8, which corresponds to approximate plume ages of 0.15-0.75 seconds (Figure 1a). Three different fuels and three different engine thrust conditions were investigated. The thrust conditions bracket the range of realistic flight conditions on the DC-8 flight curve, which describes the

relationship between engine fuel burn (proportional to thrust) and airspeed for a given aircraft weight and cruise altitude (Figure 1d). Commercial aircraft typically fly at thrust conditions at or slightly above the Maximum Range point, which corresponds to where aircraft drag is minimized, but thrust can be operationally varied by the flight crew based on schedule and fuel burn considerations.

The use of the four-engine DC-8 is quite advantageous for in-flight engine emissions testing and overcomes sampling challenges associated with using multiple fuels and thrust conditions in dual-engine flight tests for two reasons. First, the thrust settings of the two inboard engines (#2 and #3) can be varied over the range of reasonable flight operating conditions while adjusting the outboard engines (#1 and #4) to maintain a constant airspeed. Figure 1d shows three ACCESS-2 engine thrust settings (blue points) that were set at an achievable operating speed of 0.6 Mach for the NASA and DLR chase planes. Second, we can investigate both fuels on both engines during a single flight by adjusting the valves in the fuel cross feeds in order to account for differences in engine performance that influence the engine-specific emissions indices. For example, the DC-8 left inboard engine emits more particles than the right inboard engine.

The effect of thrust changes on engine emissions of particles and, particularly water vapor, is visibly evident under contrail-forming conditions, where the plume is supersaturated with respect to liquid water, satisfying the Schmidt-Appleman criterion (*28–30*). Conditions encountered during ACCESS did not always warrant contrail formation, and increased ultrafine particle concentrations were measured under clear air conditions, which implies substantial ice particle scavenging of these small, nucleation-mode particles. Consequently, for the purposes of this report, we confine our analysis to the determination of engine emissions indices for clear air (i.e., non-contrail-forming) exhaust plumes only. This ensures that the reported emissions data are not affected by contrail-processing in between the engine exhaust plane and the sampling inlet.

Particle number and mass concentrations, as well as trace gas concentrations of carbon dioxide (CO_2), carbon monoxide (CO), and nitrogen oxides (NO_X), were sampled by the chase aircraft through sample inlets mounted on the crown of the DLR and NASA Falcon chase aircraft and below-wing-mounted instruments on the NRC T-33. The amount of a given species emitted per kg of fuel burn is the species emissions index (EI) and was computed as described in the SOM.

Table 1 shows the geometric mean ($\overset{\times}{\div}$ one geometric standard deviation) particle and trace gas EIs for multiple penetrations of the #3 engine exhaust plume, while it was operating at medium cruise thrust (corresponding to Maximum Range in Figure 1d). EI summary statistics for the additional thrust conditions and the #2 engine are tabulated in the SOM. Particle number EIs for the traditional petroleum-based jet fuels are on the order of 10^{14}-10^{15} kg-fuel^{-1}, with the non-volatile number EI closer to 10^{14} kg-fuel^{-1} and black carbon (BC) equivalent mass EI near 15 mg kg-fuel^{-1}. These EIs, particularly those for the non-volatile particles, fall towards the lower end of previously reported EIs from previous flight test experiments conducted during the 1990s (*31–35*), which is attributable to efficiency gains implemented in the relatively newer CFM56-2C engines. Sulfur doping of the low-sulfur Jet A from 22$\pm$13 ppmM to 416$\pm$37 ppmM had no discernible impact on the engine particle emissions for particle diameters exceeding 10 nm (the lowest detectable size in this study); however, it is known that changes in fuel sulfur content affect the total number EI by dramatically increasing the number of sub-5-nm-diameter particles (*36*). Measurements of such small particles are challenging and the results can be confounded by additional factors including the plume age and instrumental detection efficiencies (*35*).

We also tabulate EIs for the 50:50 blend of HEFA biojet fuel and low-sulfur Jet A in Table 1 and the SOM, which show a marked, approximately two-fold reduction in both volatile- and non-volatile number emissions as compared to the medium- and low-sulfur Jet A fuels. These

dramatic emissions reductions are consistent across each of the investigated engine thrust conditions (Figure 2), although the number EI reduction is slightly less pronounced at the high engine thrust setting. Ground-based tests of low-sulfur and low-aromatic Fischer-Tropsch and HEFA fuels on the NASA DC-8 engines show a similar trend with the largest particle EI reductions observed at mid-range fuel flow rates and lower particle EI reductions observed at the highest fuel flow rates in those tests (*21, 22*). However, differences in engine performance characteristics (e.g., fuel-air ratio, maximum fuel flow rate, inlet temperature and pressure) between surface tests and in-flight tests preclude a direct comparison of EIs, despite a number of promising approximation methods to use ground-based data to estimate cruise emissions inventories (*10, 37, 38*). The greatest impact on emissions is associated with a reduction in BC-equivalent mass with the biofuel blend exhibiting emissions that are 30-40% of those seen for the traditional, petroleum-based Jet A fuels.

Measured particle size distributions help to explain the differences between number and mass (volume) EIs for the two fuels as shown in Figure 3. The pronounced decrease in both total and non-volatile particle number and volume associated with the biofuel blend is apparent, as well as a slight shift in the mode peak diameter by 3-5 nm toward smaller sizes for the number distributions and 9-12 nm for the volume distributions. This shift appears to be caused by a greater reduction in the number of larger, soot mode aerosols, which serve as condensation nuclei for semi- and non-volatile organic species and sulfuric acid. Since gas-to-particle condensation scales with particle surface area (i.e., diameter-squared), the lower soot emissions from the biojet fuel blend suppress the condensational sink, which in turn, enhances the nucleation of new particles in a compensating manner. This competition manifests itself as the lop-sided, size-dependent number emissions reductions observed in the left panels of Figure 3.

We find that blending of traditional petroleum-based fuels with a HEFA biojet fuel significantly reduces the volatile and non-volatile particle emissions at real-world cruise conditions,

with comparatively minor reductions in CO observed at one of the three engine thrust conditions. Despite these 2-3-fold emissions reductions, the soot particle number EIs remain in the range of $\sim 10^{14}$ kg-fuel^{-1}; Kärcher et al. describe this condition as squarely within the soot-rich regime, where the number of contrail ice particles scales proportionally with the soot number EI and ambient and ultra-fine particles are unlikely to contribute meaningfully to contrail formation (*4*). Consequently, we expect the soot particle emissions reductions form biofuel blending to translate directly into reduced contrail ice crystal density.

Understanding the implications of these findings for future aviation effects on climate is challenging due to the complex interplay between direct climatic impacts of sulfate, nitrate, and BC soot emissions and their role in forming linear contrails and contrail-induced cirrus clouds. The direct radiative impacts of sulfate and nitrate aerosols are thought to be cooling, while BC, linear contrails, and contrail cirrus are thought to be warming (*1*). The FAA-sponsored Aviation Climate Change Research Initiative (ACCRI) recently evaluated the direct and indirect aviation effects on climate in an ensemble modeling study (*6*). They assumed a cruise-altitude BC mass EI of 30 mg kg-fuel^{-1} and a number EI of 2×10^{14} kg-fuel^{-1}; these values are consistent with the observed EIs in this report for the medium-sulfur Jet A at a thrust setting between the medium and high thrust test conditions. For present-day conditions (based on year 2006 traffic data), they uncovered a weak direct global radiative forcing associated with aviation BC emissions (0.6-1.0 mW m^{-2}) and stronger radiative forcings (and greater uncertainties) associated with sulfate and nitrate (-7.0 to -14.5 mW m^{-2} combined), linear contrails (2.9-11.3 mW m^{-2}), and contrail cirrus (2.9-11.3 and 12.4-51.3 mW m^{-2}). The regional forcing for the northern hemisphere is even greater, owing to the high density of air traffic north of the equator (*6*). Widespread adoption of biojet fuel blends with near-zero fuel sulfur and reduced aromatic species in the future will serve to decrease the minor direct warming associated with BC and the direct cooling associated with sulfate aerosols. It remains to be seen, however, if the reduced soot EIs and expected contrail

ice density reduction translate into a meaningful change in the cloud forcing or lifetime. A critical first step is the determination of the number and size of engine exhaust particles at cruise conditions, for which data are non-existent for for engines burning biojet fuel blends and sparse even for conventional, petroleum-based fuels (*4*). This work provides the key aerosol microphysical parameters needed by transportation and climate modeling efforts to constrain future aviation impacts on the environment as the fleet transitions to toward widespread adoption of aviation biofuels.

References and Notes

1. D. S. Lee, *et al.*, *Atmospheric Environment* **44**, 4678 (2010).

2. M. Tesche, P. Achtert, P. Glantz, K. J. Noone, *Nature Communications* **7**, 12016 (2016).

3. U. Burkhardt, B. Kärcher, *Nature Climate Change* **1**, 54 (2011).

4. B. Kärcher, U. Burkhardt, A. Bier, L. Bock, I. Ford, *Journal of Geophysical Research – Atmospheres* **120** (2015).

5. J. Hendricks, B. Kärcher, U. Lohmann, M. Ponater, *Geophysical Research Letters* **32**, L12814 (2005).

6. G. P. Brasseur, *et al.*, *Bulletin of the American Meteorological Society* pp. 561–583 (2016).

7. A. Gettelman, C. Chen, *Geophysical Research Letters* **40**, 2785 (2013).

8. X. Liu, J. E. Penner, M. Wang, *Journal of Geophysical Research* **114**, D03204 (2009).

9. A. Petzold, *et al.*, *Atmospheric Chemistry and Physics* **5**, 3187 (2005).

10. M. E. Stettler, A. M. Boies, A. Petzold, S. R. Barrett, *Environmental Science and Technology* **47**, 10397 (2013).

11. EU, Directive 2008/101/EC of the European Parliament and of the Council of 19 November 2008 amending Directive 2003/87/EC so as to include aviation activities in the scheme for greenhouse gas emission allowance trading within the Community (2008).

12. US C.F.R. Vol. 80, No. 126, Proposed Finding That Greenhouse Gas Emissions From Aircraft Cause or Contribute to Air Pollution That May Reasonably Be Anticipated To Endanger Public Health and Welfare and Advance Notice of Proposed Rulemaking (2015).

13. US EPA, Fact Sheet: EPA takes first steps to address GHG emissions from aircraft engines (2015).

14. J. Ringbeck, V. Koch, *Biofuels* **1**, 519 (2010).

15. Realising Europe's Vision for Aviation: Strategic Research & Innovation Agenda (Executive Summary), *Tech. rep.*, Advisory Council for Aviation Research and Innovation in Europe (ACARE) (2012).

16. L. Rye, S. Blakey, C. Wilson, *Energy & Environmental Science* **3**, 17 (2010).

17. B. Warshay, J. Pan, S. Sgouridis, *Biofuels* **2**, 33 (2011).

18. N. Savage, *Nature* **474**, S9 (2011).

19. E. Corporan, *et al.*, *Energy & fuels* **21**, 2615 (2007).

20. P. Lobo, D. E. Hagen, P. D. Whitefield, *Environmental science & technology* **45**, 10744 (2011).

21. A. J. Beyersdorf, *et al.*, *Atmospheric Chemistry and Physics* **14**, 11 (2014).

22. R. H. Moore, *et al.*, *Energy & Fuels* **29**, 2591 (2015).

23. C. A. Moses, P. N. Roets, *Journal of Engineering for Gas Turbines and Power* **131**, 041502 (2009).

24. E. Corporan, *et al.*, *Energy & Fuels* **25**, 955 (2011).

25. M. J. DeWitt, E. Corporan, J. Graham, D. Minus, *Energy & Fuels* **22**, 2411 (2008).

26. ASTM D1655: Standard specificiation for aviation turbine fuels, ASTM International. http://www.astm.org/Standards/D1655.htm.

27. ASTM D7566: Standard specificiation for aviation turbine fuel containing synthesized hydrocarbons, ASTM International. http://www.astm.org/Standards/D7566.htm.

28. E. Schmidt, *Schriften det Deutschen Akademie der Luftfahrt-forschung* (Oldenbourg, 1941), vol. 44, chap. Die Entstehung von Eisnebel aus den Auspuffgasen von Flugmotoren, pp. 1–22.

29. H. Appleman, *Bulletin of the American Meteorological Society* **34**, 14 (1953).

30. U. Schumann, *et al.*, *Journal of Geophysical Research* **101**, 6853 (1996).

31. B. E. Anderson, *et al.*, *Geophysical Research Letters* **25**, 1689 (1998).

32. F. Schröder, *et al.*, *Geophysical Research Letters* **25**, 2789 (1998).

33. O. B. Toon, R. C. Miake-Lye, *Geophysical Research Letters* **25**, 1109 (1998).

34. A. Petzold, A. Döpelheuer, C. Brock, F. Schröder, *Journal of Geophysical Research: Atmospheres (1984–2012)* **104**, 22171 (1999).

35. U. Schumann, *et al.*, *Journal of Geophysical Research: Atmospheres (1984–2012)* **107**, AAC (2002).

36. C. A. Brock, *et al.*, *Journal of Geophysical Research* **105**, 26,555 (2000).

37. A. Petzold, A. Döpelheuer, *Aerosol Science and Technology* **29**, 355 (1998).

38. J. Peck, O. O. Oluwole, H.-W. Wong, R. C. Miake-Lye, *Journal of the Air & Waste Management Association* **63**, 367 (2013).

39. We thank the flight crew of the NASA DC-8. This work was supported by the NASA Advanced Air Vehicles Program, Advanced Air Transport Technology Project. RHM was supported by a NASA Postdoctoral Program fellowship.

Table 1: Summary table of emissions indices measured in clear air at the medium thrust cruise condition. Data are for the right inboard engine (#3) at altitudes between 30,000 and 36,000 ft. Data for other thrust settings are included in the SOM.

	Medium Sulfur Jet A	**Low Sulfur Jet A**		**50:50 HEFA – Low Sulfur Jet A Blend**	
Emissions Index Parameter (per kg fuel)	**Emission Index†**	**Emission Index†**	**Ratio**	**Emission Index†**	**Ratio**
Total Particle Number ($D_p > 5$ nm)	-	1.94×10^{15} $\overset{\times}{\div}$ 1.53	-	1.58×10^{15} $\overset{\times}{\div}$ 1.64	-
Ultrafine Particle Number ($5 < D_p < 10$ nm)	-	1.40×10^{15} $\overset{\times}{\div}$ 1.62	-	1.24×10^{15} $\overset{\times}{\div}$ 1.74	-
Fine Particle Number ($D_p > 10$ nm)	6.51×10^{14} $\overset{\times}{\div}$ 1.14	7.01×10^{14} $\overset{\times}{\div}$ 1.55	1.08	3.36×10^{14} $\overset{\times}{\div}$ 1.33	**0.52****
Volatile Fine Particle Number	3.86×10^{14} $\overset{\times}{\div}$ 1.08	3.52×10^{14} $\overset{\times}{\div}$ 1.74	0.91	1.86×10^{14} $\overset{\times}{\div}$ 1.38	**0.48****
Non-Volatile Fine Particle Number	2.63×10^{14} $\overset{\times}{\div}$ 1.26	3.43×10^{14} $\overset{\times}{\div}$ 1.39	1.30	1.46×10^{14} $\overset{\times}{\div}$ 1.37	**0.55****
Total Particle Volume ($5 < D_p < 120$ nm) (mm^3)	16.58 $\overset{\times}{\div}$ 1.14	18.03 $\overset{\times}{\div}$ 1.85	1.09	8.62 $\overset{\times}{\div}$ 1.72	0.52
Volatile Particle Volume (mm^3)	5.62 $\overset{\times}{\div}$ 1.67	5.98 $\overset{\times}{\div}$ 1.86	1.06	2.90 $\overset{\times}{\div}$ 1.88	0.52
Non-Volatile Particle Volume (mm^3)	10.65 $\overset{\times}{\div}$ 1.11	12.03 $\overset{\times}{\div}$ 1.85	1.13	5.42 $\overset{\times}{\div}$ 1.73	**0.51****
PSAP BC-Equivalent Mass at 467 nm (mg)	17.12 $\overset{\times}{\div}$ 1.12	14.48 $\overset{\times}{\div}$ 1.24	0.85	7.24 $\overset{\times}{\div}$ 1.33	**0.42****
PSAP BC-Equivalent Mass at 530 nm (mg)	16.85 $\overset{\times}{\div}$ 1.12	12.89 $\overset{\times}{\div}$ 1.36	0.76	6.79 $\overset{\times}{\div}$ 1.33	**0.40****
PSAP BC-Equivalent Mass at 660 nm (mg)	16.15 $\overset{\times}{\div}$ 1.13	16.07 $\overset{\times}{\div}$ 1.16	0.99	6.01 $\overset{\times}{\div}$ 1.39	**0.37****
Carbon Monoxide, CO (g)	5.99 ± 0.96	4.02 ± 0.54	**0.67****	4.68 ± 1.27	**0.78***
Nitrogen Oxides, NO_x (g)	7.26 ± 0.50	7.60 ± 0.41	1.05	7.28 ± 0.33	1.00
Number of Plume Intercepts	4	5		10	

Significance Level: **** $p < 0.001$, *** $p < 0.01$, ** $p < 0.05$, * $p < 0.1$

†Particle EIs are reported as the geometric mean $\overset{\times}{\div}$ the geometric standard deviation, while trace gas EIs are reported as the arithmetic mean $\pm$ the arithmetic standard deviation.

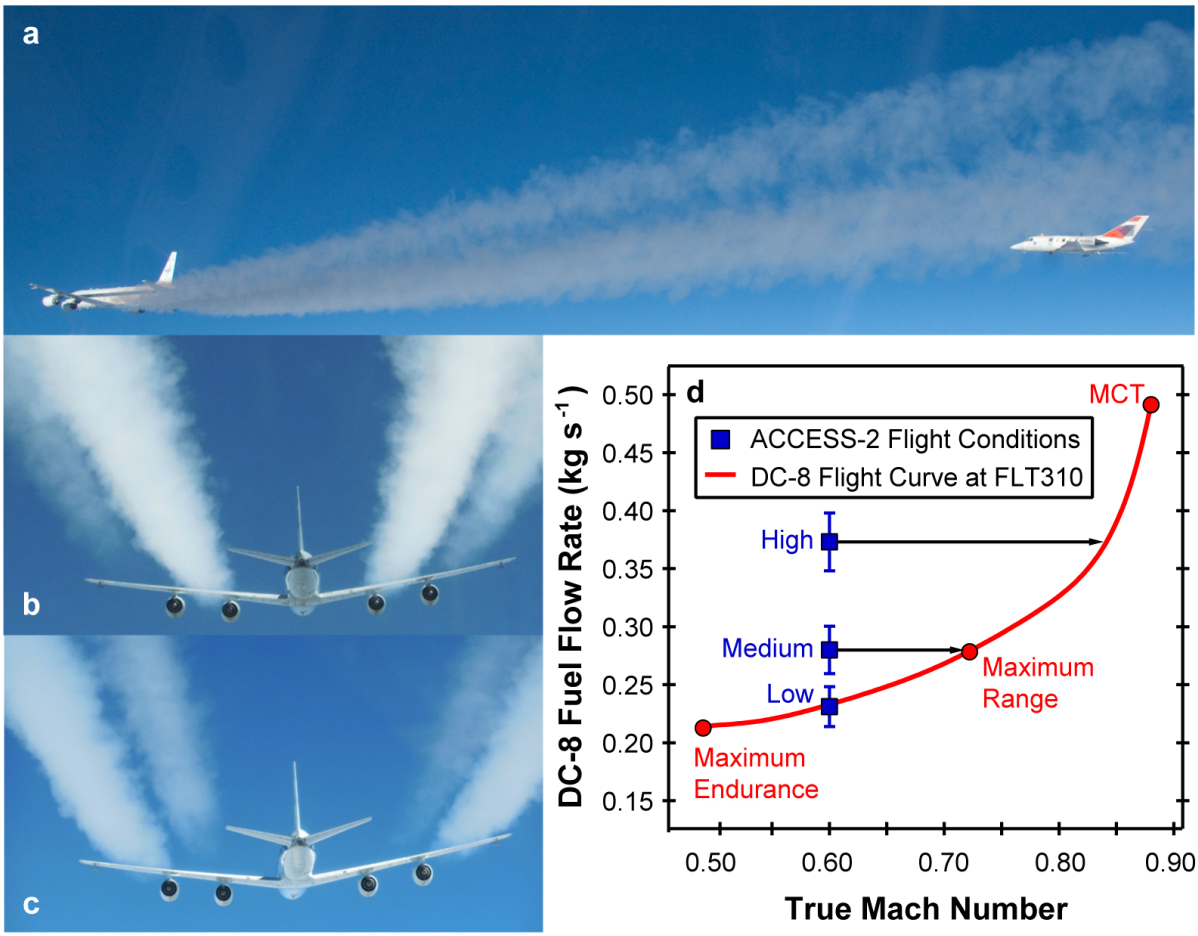

Figure 1: Side view of the NASA HU-25 Falcon aircraft sampling the DC-8 contrail (a). Also shown are forward views of the DC-8 contrails with the inboard engines throttled up to maximum continuous thrust (MCT) and the outboard engines throttled back (b), and the reverse conditions (c). The operational flight curve for the DC-8 is shown as the red curve in (d) assuming an average aircraft gross weight of 200,000 lbs. The blue points correspond to the ACCESS-2 engine thrust settings. Note that all EIs reported in this manuscript are for clear air (i.e., non-contrail-forming conditions).

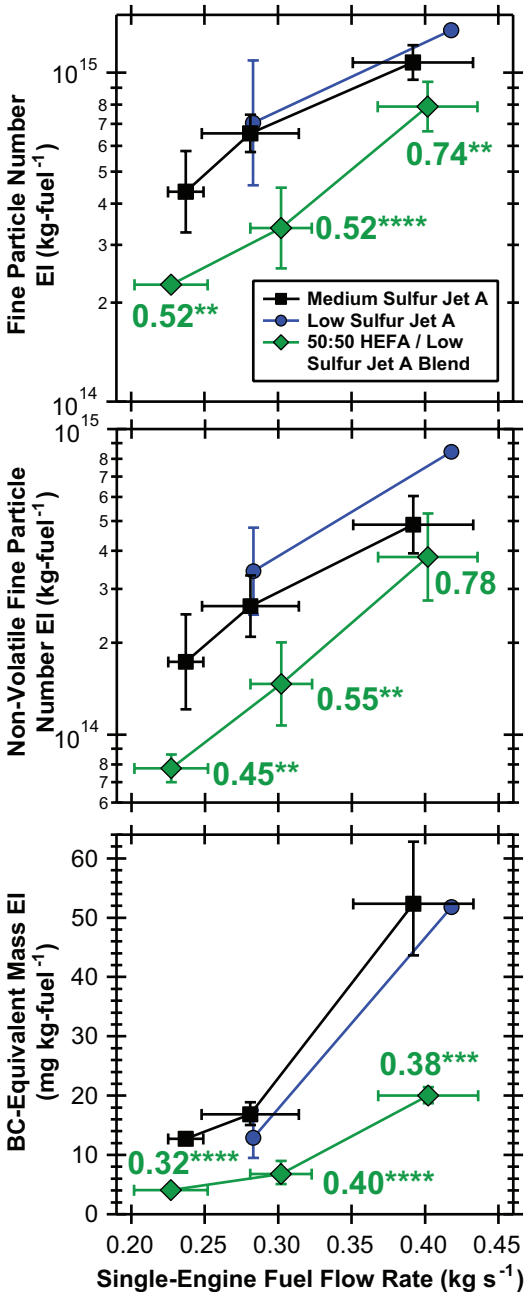

Figure 2: Geometric mean particle emissions indices ($\overset{\times}{\div}$ one geometric standard deviation) for all thrust settings and each fuel burned on the right inboard engine (#3) at altitudes between 30,000 and 36,000 ft. The ratio of the EIs for the 50:50 biofuel blend and the medium sulfur Jet A are denoted beside each point with the number of stars denoting the statistical significance level as given in Table 1 and in the SOM.

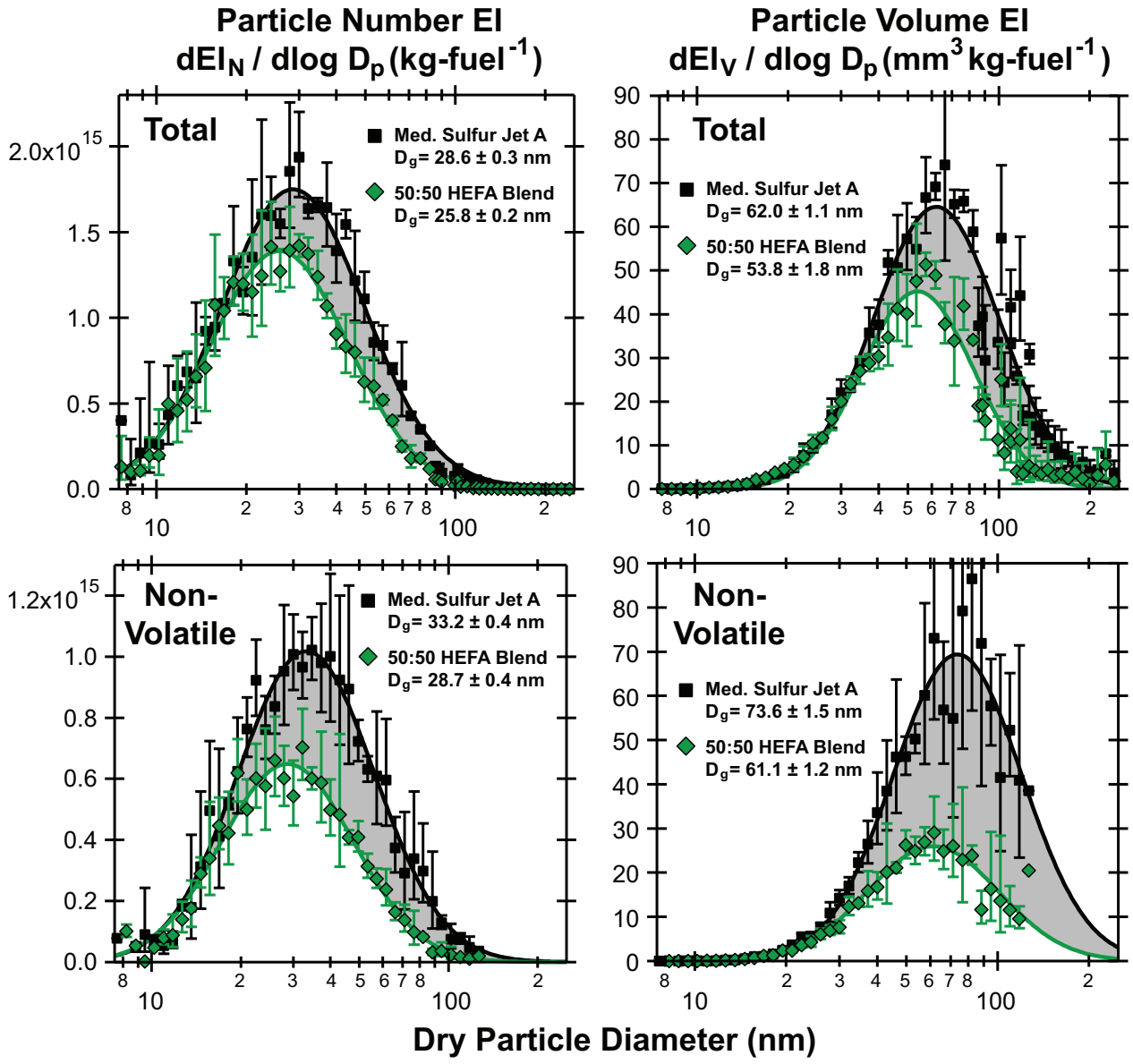

Figure 3: Particle number (left) and volume (right) EI size distributions for the total (top) and non-volatile fraction (bottom) measured at the high thrust condition behind the #3 engine. Points are geometric means and error bars are the geometric standard deviation (N = 4 and 6 for the High Sulfur Jet A and 50:50 Low Sulfur Jet A – HEFA blend, respectively). Solid lines are lognormal fits and the shaded area represents the difference between the two curves. The geometric mean diameter for each fit are denoted in the legend, while all fit parameters are given in the SOM.

Supporting Online Material for *Biofuel blending reduces aircraft engine particle emissions at cruise conditions*

Richard H. Moore,[1*] Kenneth L. Thornhill,[1,2] Bernadett Weinzierl,[3,4]
Daniel Sauer,[3,4], Eugenio D'Ascoli,[3,4] Brian Beaton,[1]
Andreas J. Beyersdorf,[1] Dan Bulzan,[6] Chelsea Corr,[1,5]
Ewan Crosbie,[1,5] Robert Martin,[1] Dean Riddick,[1]
Michael Shook,[1,2] Gregory Slover,[1] Christiane Voigt,[3]
Robert White,[1] Edward Winstead,[1,2] Richard Yasky,[1]
Luke D. Ziemba,[1] Anthony Brown,[7] Hans Schlager,[3]
and Bruce E. Anderson[1]

[*]To whom correspondence should be addressed;
E-mail: richard.h.moore@nasa.gov.

Included in this document:

S1 Materials and Methods

S1.1 Source Aircraft and Engines

The NASA DC-8 (Tail Number N817NA) and its four, CFM56-2C-1 engines have been previously described in detail elsewhere (*1–5*). The engines were installed on the airframe in 1986 and are maintained in accordance with the CFM56-2C and Douglas DC-8 maintanance manuals and inspection task cards. Given the use of the aircraft as a NASA flying laboratory, the annual flight hours for the aircraft and engines are typically low as compared to commercial aircraft.

S1.2 Jet Fuel Properties

The relevant chemical and physical properties of the investigated fuels are summarized in Table S1. Testing was performed by the U.S. Air Force Petroleum Agency laboratory at Wright-Patterson Air Force Base. Samples were drawn from the left inboard (#2) fuel tank of the DC-8 before each flight and from the fuel truck before uploading the HEFA blend onto the DC-8. Tests conform to standard methods for fuel sulfur (ASTM D2622), aromatics (ASTM D1319), hydrogen content (ASTM D7171), naphthalenes (ASTM D1840), density (ASTM D4052), and net heat of combustion (ASTM D3338).

Table S1: Mean fuel properties ($\pm$ one standard deviation) for each of the three, investigated fuels. Samples were obtained prior to each flight from the fuel truck or DC-8 fuel tanks.

Fuel Property	**Medium Sulfur Jet A**	**Low Sulfur Jet A**	**50:50 HEFA – Low Sulfur Jet A Blend**	**Jet A Specification Range**[†]
Sulfur (ppmM)	416 ± 37	22 ± 13	11 ± 3	<3000
Aromatics (volume%)	21.1 ± 0.7	21.4 ± 1.4	12.9 ± 1.2	8–25
Hydrogen Content (mass%)	13.6 ± 0.3	13.8 ± 0.2	14.7 ± 0.2	>13.4
Naphthalenes (volume%)	0.9 ± 0.2	1.0 ± 0.2	0.4 ± 0.0	<3.0
Density (kg m^{-3})	809.2 ± 1.8	810 ± 0.5	787.4 ± 2.5	775–840
Net Heat of Combustion (MJ kg^{-1})	43.14 ± 0.05	43.15 ± 0.06	43.52 ± 0.04	>42.8
Number of Samples Tested	5	4	5	

[†] ASTM D1655 and D7566

S1.3 Particle and Trace Gas Measurements

Measurements were made from the NASA HU-25 Falcon aircraft using the NASA Langley Aerosol Research Group (LARGE) suite of in-situ instruments, which have been used for numerous airborne research campaigns as described elsewhere (*14–16*). Similarly, the instruments aboard the DLR Falcon 20 and NRC-Canada T-33 aircraft are well-characterized with long flight heritage. Results from the following instruments were used in this study. Total particle number concentration ($D_{\mathrm{P}} > 5$ nm) were measured by a custom condensation particle counter (CPC) onboard the DLR Falcon 20. Fine particle number concentration ($D_{\mathrm{P}} > 10$ nm) was measured by a pair of TSI 3010 CPCs on the HU-25; one of the CPCs measured the non-volatile particle fraction after sample treatment with a thermaldenuder at 350°C, while the other measured the total (volatile + non-volatile) aerosol number. Similarly, total and non-volatile particle size distributions were measured by a TSI nano Scanning Mobility Particle Sizer (nanoSMPS; 3936, 3085, 3025A) for undenuded and denuded sample streams, respectively. Because the nanoSMPS requires 45 seconds to complete a size upscan, a dual lag chamber system was employed, where two cylinders were charged at high flow rate (19 L min^{-1}) while the aircraft was sampling the exhaust plume. These lag chambers were then sampled by the nanoSMPS at 1.5 L min^{-1}. The upper portion of the size distribution ($D_{\mathrm{P}} > 85$ nm) was measured by an ultra-high sensitivity aerosol size spectrometer (UHSAS; Droplet Measurement Technologies), which was calibrated using soot particles from a Mini-CAST soot generator that were size-classified with a differential mobility analyzer (*17*). The nanoSMPS size distributions were integrated to yield the total and non-volatile particle volume. Finally, particle black carbon (BC) equivalent mass at three different optical wavelengths were measured by a Radiance Research Particle Soot Absorption Photometer (PSAP). The PSAP mass concentrations were corrected for filter scattering artifacts following Virkkula, 2010 (*18*), assuming a single scattering albedo (SSA) of 0.1, which is consistent with Mie theory calculations using the measured size distribution and a BC refrac-

tive index of 1.95-0.75i (*19*). The PSAP correction is weakly sensitive to this assumed SSA and varies by only 1% over the SSA range of 0.03-0.3.

Trace gas carbon dioxide (CO_2), carbon monoxide (CO), and nitrogen oxide (NO_x concentrations were measured using Los Gatos Research instruments. CO and CO_2 were measured via cavity enhanced absorption. To measure NO_x, the sample stream was mixed with excess ozone to convert NO to NO_2, which was measured via cavity ring down spectroscopy.

S1.4 Emissions Index Calculation

As the Falcon sampling probe traverses the DC-8 engine exhaust it encounters varying concentrations of particles and trace gases due to the spatial heterogenity of the plume. Making sense of these time-varying quantities requires that we normalize them to the rate of fuel burned by the engines to arrive at an averaged emissions index (EI) across the plume. The EI of particle or trace gas species X is determined as

$$\mathrm{EI_X} = \frac{\Delta \mathrm{X} \cdot S}{\Delta \mathrm{CO_2}} \left(\mathrm{EI_{CO_2}}\right) \tag{1}$$

$$\text{where, } \mathrm{EI_{CO_2}} = \frac{RT}{PV_m} \frac{M_{\mathrm{CO_2}}}{(M_{\mathrm{C}} + \alpha M_{\mathrm{H}})} \sim 3160 \text{ gCO}_2 \text{ kg-fuel}^{-1}; \tag{2}$$

$$S\left(\mathrm{X}\right) = \begin{cases} \text{particles} : V_m / M_{\mathrm{CO_2}} \\ \text{trace gases} : M_{\mathrm{X}} / M_{\mathrm{CO_2}}; \end{cases} \tag{3}$$

ΔX and ΔCO_2 are the dilution-corrected, background-subtracted peak areas of the measured concentrations of species X and CO_2 at STP, respectively; $\mathrm{EI_{CO_2}}$ is the emissions index of CO_2, assuming the carbon content in the fuel is constant and is completely converted to CO_2; S is a unit conversion scaling factor for particle concentrations (number or mass per air volume STP) or trace gas concentrations (ppmV); R is the ideal gas constant; T is the temperature at STP (273.15 K); P is the pressure at STP (1 atm); V_m is the molar volume of ideal gas at STP (22.4

L mol^{-1}); α is the fuel hydrogen-to-carbon molar ratio; and M_X, M_{CO_2}, M_C, M_H are the molar masses of species X, CO_2, carbon, and hydrogen, respectively. Values of α calculated from Table S1 for the Jet A fuels and the blended fuel are 1.92 and 2.07, respectively; however, for this analysis, we assume a constant value of 1.92 for simplicity. This assumption introduces insignificant error ($\sim$1%) into reported EIs as compared to the measurement uncertainties.

S1.5 Particle Sampling and Transmission Loss Corrections

The size-dependent inlet aspiration efficiency of the HIMIL inlet and particle losses to the sampling lines are estimated using the Particle Loss Calculator (*20*), which accounts for diffusional, inertial, and sedimentation losses. Particles were sampled at a flow rate of 37 L min^{-1} through a 4.35 mm tube assumed to be oriented parallel to the air flow around the aircraft (mean air velocity $\sim$200 m s^{-1}). In reality, the inlet tube is shrouded, which ensures parallel sampling streamlines, but which reduces the local air velocity by an unknown amount. The sensitivity of the inlet aspiration efficiency to airspeed is, however, negligible for the ultrafine particles sampled during ACCESS. The sample then passed through approximately 0.34 m of 4.35 mm ID tubing and approximately 4 m of 7.9 mm ID tubing before being sampled by the instrumentation in the chase plane cabin. Figure S1 shows the computed, size-dependent sampling efficiency, which is used to correct the measured size distributions (Figure 3 in the main text, Figures S2-S3, and the coefficients in Table S2-S3). Given the large corrections ($\sim$40%) at the lowest particle sizes and uncertainties in the size distributions across all fuels and engine thrust conditions, we choose not to apply these corrections to the tabulated integrated number, volume, and mass emissions indices (Table 1 in the main text and Tables S5-S9) following Beyersdorf et al. (*4*) and instead focus on the differences in the sampled emissions indices across fuel types and engine powers for which the sampling characteristics and efficiency should be nearly the same.

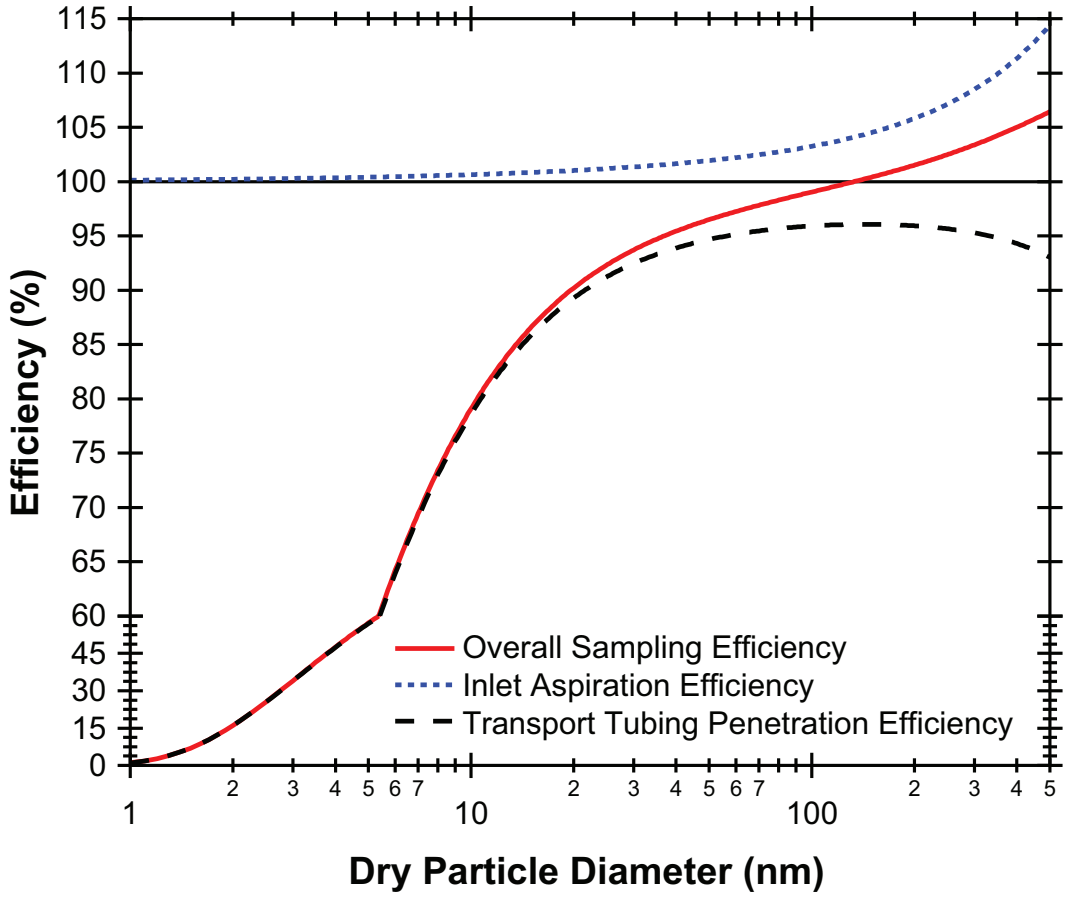

Figure S1: The overall size-dependent sampling efficiency of the HU-25 sampling system. This efficiency is the combination of inlet sampling effects (i.e., aspiration efficiency) and particle losses within the tubing between the inlet and the instruments (i.e., transport tubing penetration efficiency).

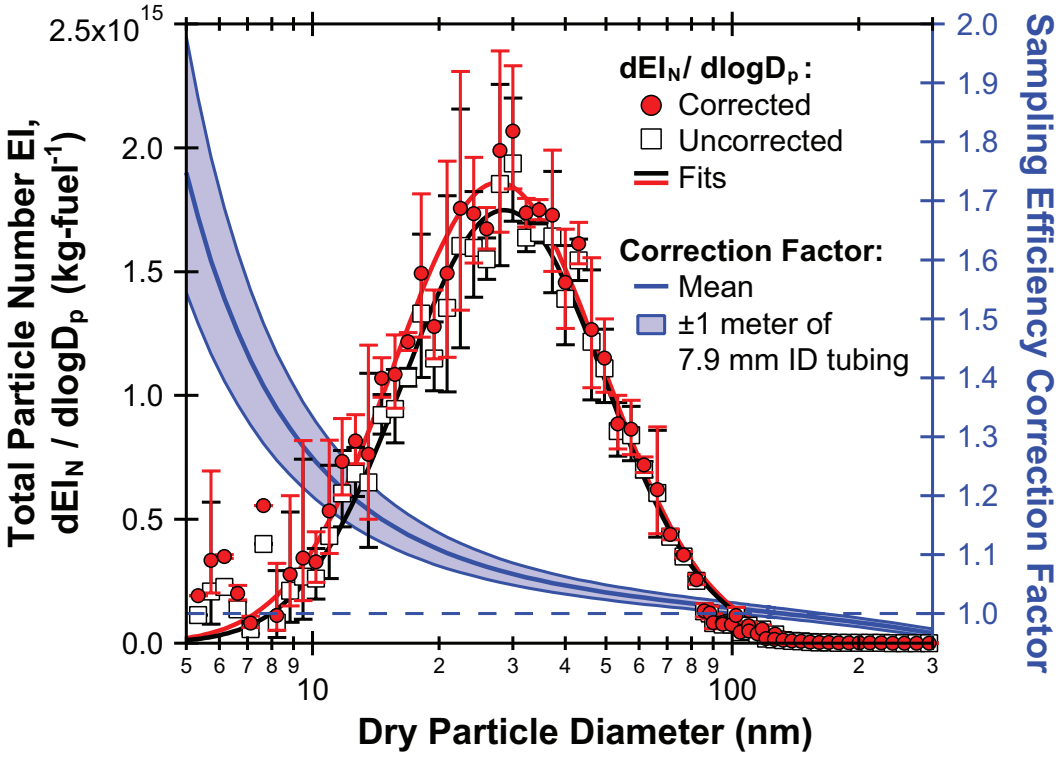

Figure S2: Total particle number size distribution both uncorrected (open squares) and corrected for the size-dependent sampling efficiency shown in Figure S1. The blue trace indicates the correction factor applied to the distribution, with the shaded region providing an indication of the sensitivity of the correction factor to variation in the transport tubing lengths, as aircraft payload integration constraints require that that the instruments be spaced throughout the cabin.

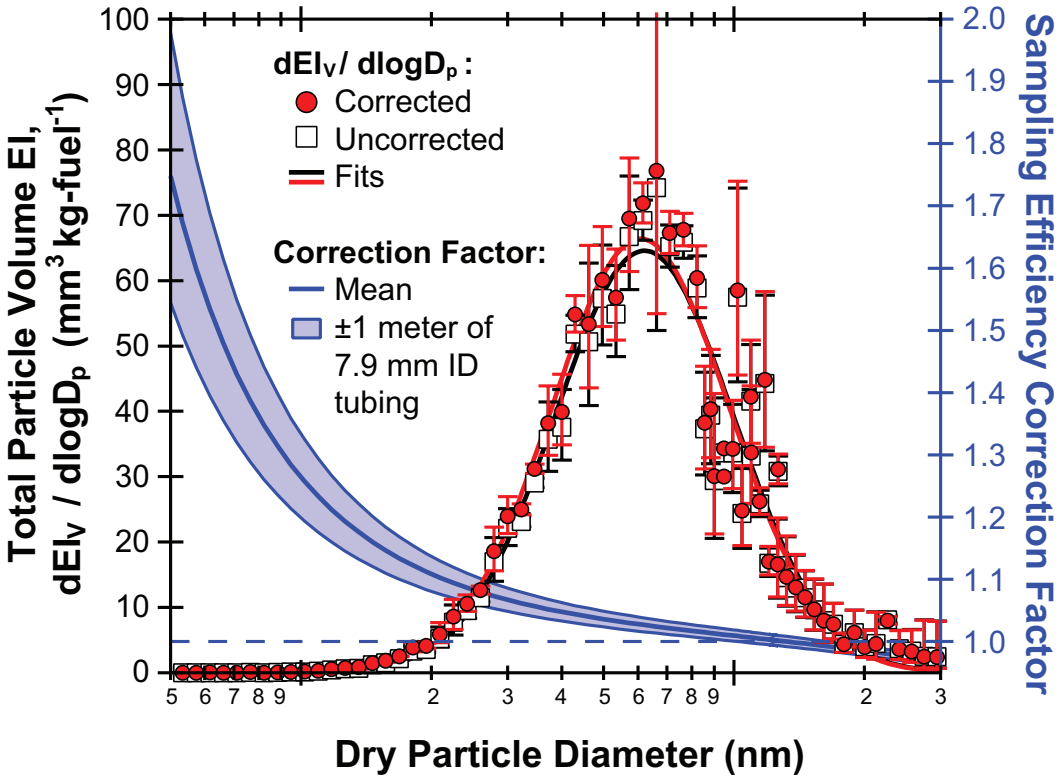

Figure S3: Total particle volume size distribution both uncorrected (open squares) and corrected for the size-dependent sampling efficiency shown in Figure S1. The blue trace indicates the correction factor applied to the distribution, with the shaded region providing an indication of the sensitivity of the correction factor to variation in the transport tubing lengths, as aircraft payload integration constraints require that that the instruments be spaced throughout the cabin.

S2 Particle Size Distribution Lognormal Fit Parameters

Particle number and volume size distributions (5-300 nm diameter) measured by the SMPS and UHSAS were fit using a single-mode, lognormal function of the form

$$\frac{dEI_{\mathrm{X}}}{d\log D_{\mathrm{P}}} = \frac{X}{\sqrt{2\pi}\log\sigma_{\mathrm{g,X}}}\exp\left[-\frac{\left(\log D_{\mathrm{P}} - \log D_{\mathrm{g,X}}\right)^2}{2\log^2\sigma_{\mathrm{g,X}}}\right] \tag{4}$$

where X is the total particle number (N) or volume (V), EI_{X} is the corresponding emissions index, D_{P} is the particle dry diameter, $D_{\mathrm{g,X}}$ is the geometric mean diameter, and $\sigma_{\mathrm{g,X}}$ is the geometric standard deviation. Fit coefficients are given for the number size distributions in Table S2 and for the volume size distributions in Table S3. All size distributions have been corrected for particle sampling and transmission losses as in Section S1.5.

Table S2: Lognormal fit coefficients (± one standard deviation) to the geometric mean particle number size distributions measured behind the left and right inboard engines (#2 and #3, respectively) at altitudes between 30,000 and 35,000 ft.

	Medium SulfurJet A			50:50 HEFA – Low Sulfur Jet A Blend		
EI Size Distribution Parameter	**N (kg fuel^{-1})**	**$D_{g,N}$ (nm)**	**$\sigma_{g,N}$**	**N (kg fuel^{-1})**	**$D_{g,N}$ (nm)**	**$\sigma_{g,N}$**
Total Particle Number, $dEI_N/dlogD_P$:						
Engine #2:						
High Engine Thrust	$(1.50\pm0.03)\times10^{15}$	29.4±0.4	1.79±0.02	$(1.09\pm0.02)\times10^{15}$	26.8±0.3	1.74±0.02
Medium Engine Thrust	$(1.07\pm0.02)\times10^{15}$	24.7±0.4	1.78±0.03	$(6.32\pm0.13)\times10^{14}$	24.0±0.3	1.69±0.02
Low Engine Thrust	$(8.28\pm0.21)\times10^{14}$	24.8±0.4	1.72±0.03	$(6.07\pm0.67)\times10^{14}$	19.3±1.8	2.09±0.21
Engine #3:						
High Engine Thrust	$(1.14\pm0.02)\times10^{15}$	27.8±0.3	1.76±0.02	$(8.77\pm0.12)\times10^{14}$	25.1±0.2	1.71±0.01
Medium Engine Thrust	$(7.01\pm0.17)\times10^{14}$	23.3±0.3	1.69±0.02	$(3.50\pm0.08)\times10^{14}$	21.5±0.3	1.73±0.03
Low Engine Thrust	$(4.68\pm0.07)\times10^{14}$	23.0±0.2	1.66±0.02	$(2.11\pm0.25)\times10^{14}$	18.6±0.9	1.43±0.08
Non-Volatile Particle Number, $dEI_N/dlogD_P$						
Engine #2:						
High Engine Thrust	$(7.64\pm0.15)\times10^{14}$	35.3±0.4	1.72±0.02	$(5.41\pm0.15)\times10^{14}$	28.7±0.5	1.75±0.03
Medium Engine Thrust	$(5.00\pm0.14)\times10^{14}$	29.7±0.5	1.64±0.03	$(2.62\pm0.07)\times10^{14}$	27.8±0.4	1.71±0.02
Low Engine Thrust	$(4.50\pm0.23)\times10^{14}$	25.5±0.9	1.86±0.07	$(4.15\pm0.63)\times10^{14}$	20.9±2.4	2.03±0.27
Engine #3:						
High Engine Thrust	$(6.30\pm0.13)\times10^{14}$	32.5±0.4	1.71±0.02	$(3.94\pm0.12)\times10^{14}$	28.0±0.5	1.68±0.03
Medium Engine Thrust	$(3.18\pm0.14)\times10^{14}$	27.0±0.7	1.63±0.04	$(1.78\pm0.06)\times10^{14}$	26.3±0.5	1.68±0.03
Low Engine Thrust	$(2.82\pm0.08)\times10^{14}$	23.5±0.5	1.73±0.03	$(1.09\pm0.08)\times10^{14}$	23.4±0.8	1.58±0.06

Table S3: Lognormal fit coefficients (± one standard deviation) to the geometric mean particle volume size distributions measured behind the left and right inboard engines (#2 and #3, respectively) at altitudes between 30,000 and 35,000 ft.

	Medium SulfurJet A			50:50 HEFA – Low Sulfur Jet A Blend		
EI Size Distribution Parameter	**V (mm^3 kg fuel^{-1})**	**$D_{g,V}$ (nm)**	**$\sigma_{g,V}$**	**V (mm^3 kg fuel^{-1})**	**$D_{g,V}$ (nm)**	**$\sigma_{g,V}$**
Total Particle Volume, $dEI_V/dlogD_P$						
Engine #2:						
High Engine Thrust	66.8±2.4	65.7±1.2	1.57±0.03	34.4±1.1	57.2±1.0	1.61±0.03
Medium Engine Thrust	28.5±0.8	57.5±0.8	1.58±0.02	14.7±0.5	52.6±0.5	1.60±0.03
Low Engine Thrust	19.9±0.6	51.9±0.8	1.59±0.02	13.0±2.3	61.6±6.0	1.67±0.19
Engine #3:						
High Engine Thrust	34.4±1.0	60.8±1.0	1.61±0.03	21.9±0.6	53.3±0.7	1.54±0.02
Medium Engine Thrust	14.4±0.6	50.4±1.0	1.51±0.03	6.7±0.5	51.9±2.2	1.73±0.08
Low Engine Thrust	8.9±0.3	48.7±0.7	1.55±0.02	3.3±0.5	49.1±5.0	1.92±0.18
Non-Volatile Particle Volume, $dEI_V/dlogD_P$						
Engine #2:						
High Engine Thrust	44.1±1.1	68.3±0.7	1.46±0.02	20.4±0.6	61.2±0.8	1.54±0.02
Medium Engine Thrust	19.6±1.1	60.9±1.8	1.57±0.05	9.7±0.5	61.5±1.6	1.66±0.05
Low Engine Thrust	15.8±0.8	64.3±1.8	1.64±0.05	8.9±2.9	58±12	1.77±0.31
Engine #3:						
High Engine Thrust	37.8±1.4	73.0±1.5	1.63±0.04	14.5±0.5	60.5±1.3	1.65±0.04
Medium Engine Thrust	12.6±1.5	66.7±5.2	1.80±0.16	6.0±0.5	61.8±3.4	1.85±0.11
Low Engine Thrust	6.1±0.3	51.8±1.1	1.56±0.03	1.9±0.2	44.9±1.8	1.57±0.07

S3 Additional Emissions Index Tables

Particle and trace gas emissions indices for the DC-8 CFM56-2C1 engines operating at three different cruise conditions are summarized in Tables S5-S9 and in Table 1 in the main text as follows:

Table S4: Summary of Emissions Index Tables

	Engine Thrust Condition		
	High	**Medium**	**Low**
Engine #2	Table S5	Table S7	Table S8
Engine #3	Table S6	Table 1 in main text	Table S9

Table S5: Summary table of emissions indices measured in clear air at the high thrust cruise condition. Data are for the left inboard engine (#2) at altitudes between 30,000 and 35,000 ft.

	Medium Sulfur Jet A	**Low Sulfur Jet A**		**50:50 HEFA – Low Sulfur Jet A Blend**	
Emissions Index Parameter (per kg fuel)	**Emission Index†**	**Emission Index†**	**Ratio**	**Emission Index†**	**Ratio**
Total Particle Number ($D_p > 5$ nm)	-	3.30×10^{15} $\overset{\times}{\div}$ 1.04	-	1.97×10^{15} $\overset{\times}{\div}$ 1.48	-
Ultrafine Particle Number ($5 < D_p < 10$ nm)	-	1.81×10^{15} $\overset{\times}{\div}$ 1.08	-	1.08×10^{15} $\overset{\times}{\div}$ 1.99	-
Fine Particle Number ($D_p > 10$ nm)	1.43×10^{15} $\overset{\times}{\div}$ 1.13	1.57×10^{15}	1.10	1.02×10^{15} $\overset{\times}{\div}$ 1.16	**0.71*****
Volatile Fine Particle Number	7.58×10^{14} $\overset{\times}{\div}$ 1.27	6.53×10^{14}	0.86	5.06×10^{14} $\overset{\times}{\div}$ 1.09	**0.67***
Non-Volatile Fine Particle Number	6.59×10^{14} $\overset{\times}{\div}$ 1.08	9.17×10^{14}	1.39	5.03×10^{14} $\overset{\times}{\div}$ 1.30	**0.76****
Total Particle Volume ($5 < D_p < 120$ nm) (mm^3)	68.23 $\overset{\times}{\div}$ 1.31	78.80	1.16	37.77 $\overset{\times}{\div}$ 1.15	0.55
Volatile Particle Volume (mm^3)	20.07 $\overset{\times}{\div}$ 1.12	29.71	1.48	15.79 $\overset{\times}{\div}$ 1.20	0.79
Non-Volatile Particle Volume (mm^3)	46.02 $\overset{\times}{\div}$ 1.55	49.09	1.07	21.65 $\overset{\times}{\div}$ 1.21	0.47
PSAP BC-Equivalent Mass at 467 nm (mg)	85.13 $\overset{\times}{\div}$ 1.12	70.49	0.83	38.94 $\overset{\times}{\div}$ 1.37	**0.46******
PSAP BC-Equivalent Mass at 530 nm (mg)	82.40 $\overset{\times}{\div}$ 1.12	67.94	0.82	37.55 $\overset{\times}{\div}$ 1.39	**0.46******
PSAP BC-Equivalent Mass at 660 nm (mg)	75.38 $\overset{\times}{\div}$ 1.12	66.43	0.88	36.84 $\overset{\times}{\div}$ 1.39	**0.49*****
Carbon Monoxide, CO (g)	5.62 ± 0.95	3.57	0.64	4.43 ± 1.17	0.79
Nitrogen Oxides, NO_x (g)	9.67 ± 0.71	-	-	9.61 ± 0.80	0.99
Number of Plume Intercepts	4	1		7	

Significance Level: **** $p < 0.001$, *** $p < 0.01$, ** $p < 0.05$, * $p < 0.1$

†Particle EIs are reported as the geometric mean $\overset{\times}{\div}$ the geometric standard deviation, while trace gas EIs are reported as the arithmetic mean $\pm$ the arithmetic standard deviation.

Table S6: Summary table of emissions indices measured in clear air at the high thrust cruise condition. Data are for the right inboard engine (#3) at altitudes between 30,000 and 35,000 ft.

	Medium Sulfur Jet A	**Low Sulfur Jet A**		**50:50 HEFA – Low Sulfur Jet A Blend**	
Emissions Index Parameter (per kg fuel)	**Emission Index†**	**Emission Index†**	**Ratio**	**Emission Index†**	**Ratio**
Total Particle Number ($D_p > 5$ nm)	-	2.11×10^{15} $\overset{\times}{\div}$ 1.23	-	1.62×10^{15} $\overset{\times}{\div}$ 1.44	-
Ultrafine Particle Number ($5 < D_p < 10$ nm)	-	1.16×10^{15} $\overset{\times}{\div}$ 1.45	-	9.15×10^{14} $\overset{\times}{\div}$ 1.12	-
Fine Particle Number ($D_p > 10$ nm)	1.07×10^{15} $\overset{\times}{\div}$ 1.13	1.34×10^{15}	1.25	7.87×10^{14} $\overset{\times}{\div}$ 1.19	**0.74****
Volatile Fine Particle Number	5.81×10^{14} $\overset{\times}{\div}$ 1.07	4.97×10^{14}	0.86	3.98×10^{14} $\overset{\times}{\div}$ 1.06	**0.69******
Non-Volatile Fine Particle Number	4.86×10^{14} $\overset{\times}{\div}$ 1.24	8.43×10^{14}	1.74	3.81×10^{14} $\overset{\times}{\div}$ 1.39	0.78
Total Particle Volume ($5 < D_p < 120$ nm) (mm^3)	44.30 $\overset{\times}{\div}$ 1.14	50.01	1.13	23.32 $\overset{\times}{\div}$ 1.14	**0.53***
Volatile Particle Volume (mm^3)	9.51 $\overset{\times}{\div}$ 1.54	13.53	1.42	9.39 $\overset{\times}{\div}$ 1.54	0.99
Non-Volatile Particle Volume (mm^3)	32.81 $\overset{\times}{\div}$ 1.34	36.48	1.11	13.27 $\overset{\times}{\div}$ 1.06	0.40
PSAP BC-Equivalent Mass at 467 nm (mg)	54.00 $\overset{\times}{\div}$ 1.20	53.55	0.99	20.84 $\overset{\times}{\div}$ 1.07	**0.39*****
PSAP BC-Equivalent Mass at 530 nm (mg)	52.38 $\overset{\times}{\div}$ 1.20	51.77	0.99	20.00 $\overset{\times}{\div}$ 1.07	**0.38*****
PSAP BC-Equivalent Mass at 660 nm (mg)	50.95 $\overset{\times}{\div}$ 1.20	50.10	0.98	19.54 $\overset{\times}{\div}$ 1.07	**0.38*****
Carbon Monoxide, CO (g)	5.18 ± 0.72	3.82	0.74	4.70 ± 1.20	0.91
Nitrogen Oxides, NO_x (g)	9.45 ± 0.49	9.77	1.03	9.03 ± 0.58	0.96
Number of Plume Intercepts	4	1		5	

Significance Level: **** $p < 0.001$, *** $p < 0.01$, ** $p < 0.05$, * $p < 0.1$

†Particle EIs are reported as the geometric mean $\overset{\times}{\div}$ the geometric standard deviation, while trace gas EIs are reported as the arithmetic mean $\pm$ the arithmetic standard deviation.

Table S7: Summary table of emissions indices measured in clear air at the medium thrust cruise condition. Data are for the left inboard engine (#2) at altitudes between 30,000 and 35,000 ft.

	Medium Sulfur Jet A	**Low Sulfur Jet A**		**50:50 HEFA – Low Sulfur Jet A Blend**	
Emissions Index Parameter (per kg fuel)	**Emission Index†**	**Emission Index†**	**Ratio**	**Emission Index†**	**Ratio**
Total Particle Number ($D_p > 5$ nm)	-	3.25×10^{15} $\overset{\times}{\div}$ 1.09	-	2.77×10^{15} $\overset{\times}{\div}$ 1.24	-
Ultrafine Particle Number ($5 < D_p < 10$ nm)	-	2.26×10^{15} $\overset{\times}{\div}$ 1.10	-	2.23×10^{15} $\overset{\times}{\div}$ 1.24	-
Fine Particle Number ($D_p > 10$ nm)	9.97×10^{14} $\overset{\times}{\div}$ 1.14	1.12×10^{15} $\overset{\times}{\div}$ 1.28	1.12	6.01×10^{14} $\overset{\times}{\div}$ 1.35	**0.60***
Volatile Fine Particle Number	5.65×10^{14} $\overset{\times}{\div}$ 1.08	4.96×10^{14} $\overset{\times}{\div}$ 1.39	0.88	3.14×10^{14} $\overset{\times}{\div}$ 1.51	**0.56****
Non-Volatile Fine Particle Number	4.28×10^{14} $\overset{\times}{\div}$ 1.26	6.13×10^{14} $\overset{\times}{\div}$ 1.23	1.43	2.79×10^{14} $\overset{\times}{\div}$ 1.27	0.65
Total Particle Volume ($5 < D_p < 120$ nm) (mm^3)	30.65 $\overset{\times}{\div}$ 1.06	37.96 $\overset{\times}{\div}$ 1.39	1.24	16.37 $\overset{\times}{\div}$ 1.54	**0.53***
Volatile Particle Volume (mm^3)	10.30 $\overset{\times}{\div}$ 1.30	15.02 $\overset{\times}{\div}$ 1.35	1.46	6.08 $\overset{\times}{\div}$ 2.10	0.59
Non-Volatile Particle Volume (mm^3)	20.03 $\overset{\times}{\div}$ 1.05	22.75 $\overset{\times}{\div}$ 1.44	1.14	9.83 $\overset{\times}{\div}$ 1.32	**0.49****
PSAP BC-Equivalent Mass at 467 nm (mg)	41.29 $\overset{\times}{\div}$ 1.18	42.40 $\overset{\times}{\div}$ 1.13	1.03	17.09 $\overset{\times}{\div}$ 1.07	**0.41*****
PSAP BC-Equivalent Mass at 530 nm (mg)	39.56 $\overset{\times}{\div}$ 1.18	41.07 $\overset{\times}{\div}$ 1.13	1.04	16.79 $\overset{\times}{\div}$ 1.10	**0.42*****
PSAP BC-Equivalent Mass at 660 nm (mg)	37.88 $\overset{\times}{\div}$ 1.20	41.45 $\overset{\times}{\div}$ 1.18	1.09	17.51 $\overset{\times}{\div}$ 1.16	**0.46*****
Carbon Monoxide, CO (g)	6.06 ± 0.66	4.06 ± 0.41	**0.67*****	5.12 ± 1.42	0.85
Nitrogen Oxides, NO_x (g)	7.53 ± 0.21	7.67 ± 0.58	1.02	7.35 ± 1.44	0.98
Number of Plume Intercepts	4	8		7	

Significance Level: **** $p < 0.001$, *** $p < 0.01$, ** $p < 0.05$, * $p < 0.1$

†Particle EIs are reported as the geometric mean $\overset{\times}{\div}$ the geometric standard deviation, while trace gas EIs are reported as the arithmetic mean $\pm$ the arithmetic standard deviation.

Table S8: Summary table of emissions indices measured in clear air at the low thrust cruise condition. Data are for the left inboard engine (#2) at altitudes between 30,000 and 35,000 ft.

	Medium Sulfur Jet A	**Low Sulfur Jet A**		**50:50 HEFA – Low Sulfur Jet A Blend**	
Emissions Index Parameter (per kg fuel)	**Emission Index†**	**Emission Index†**	**Ratio**	**Emission Index†**	**Ratio**
Total Particle Number ($D_p > 5$ nm)	-	-	-	-	-
Ultrafine Particle Number ($5 < D_p < 10$ nm)	-	-	-	-	-
Fine Particle Number ($D_p > 10$ nm)	8.61×10^{14} $\overset{\times}{\div}$ 1.27	-	-	4.39×10^{14} $\overset{\times}{\div}$ 1.04	**0.51*****
Volatile Fine Particle Number	5.19×10^{14} $\overset{\times}{\div}$ 1.23	-	-	2.48×10^{14} $\overset{\times}{\div}$ 1.00	**0.48*****
Non-Volatile Fine Particle Number	3.39×10^{14} $\overset{\times}{\div}$ 1.36	-	-	1.90×10^{14} $\overset{\times}{\div}$ 1.09	**0.56*****
Total Particle Volume ($5 < D_p < 120$ nm) (mm^3)	20.79 $\overset{\times}{\div}$ 1.19	-	-	13.13	0.63
Volatile Particle Volume (mm^3)	4.16 $\overset{\times}{\div}$ 2.18	-	-	2.13	0.51
Non-Volatile Particle Volume (mm^3)	15.61 $\overset{\times}{\div}$ 1.00	-	-	11.00	0.70
PSAP BC-Equivalent Mass at 467 nm (mg)	32.85 $\overset{\times}{\div}$ 1.07	-	-	9.53	0.29
PSAP BC-Equivalent Mass at 530 nm (mg)	31.90 $\overset{\times}{\div}$ 1.04	-	-	7.86	0.25
PSAP BC-Equivalent Mass at 660 nm (mg)	32.03 $\overset{\times}{\div}$ 1.09	-	-	9.88	0.31
Carbon Monoxide, CO (g)	8.17 ± 0.68	-	-	6.33 ± 0.25	**0.77*****
Nitrogen Oxides, NO_x (g)	6.82 ± 0.20	-	-	6.72 ± 0.12	0.98
Number of Plume Intercepts	5	0		2	

Significance Level: **** $p < 0.001$, *** $p < 0.01$, ** $p < 0.05$, * $p < 0.1$

†Particle EIs are reported as the geometric mean $\overset{\times}{\div}$ the geometric standard deviation, while trace gas EIs are reported as the arithmetic mean $\pm$ the arithmetic standard deviation.

Table S9: Summary table of emissions indices measured in clear air at the low thrust cruise condition. Data are for the right inboard engine (#3) at altitudes between 30,000 and 35,000 ft.

	Medium Sulfur Jet A	**Low Sulfur Jet A**		**50:50 HEFA – Low Sulfur Jet A Blend**	
Emissions Index Parameter (per kg fuel)	**Emission Index†**	**Emission Index†**	**Ratio**	**Emission Index†**	**Ratio**
Total Particle Number ($D_p > 5$ nm)	-	-	-	-	-
Ultrafine Particle Number ($5 < D_p < 10$ nm)	-	-	-	-	-
Fine Particle Number ($D_p > 10$ nm)	4.33×10^{14} $\overset{\times}{\div}$ 1.33	-	-	2.26×10^{14} $\overset{\times}{\div}$ 1.03	**0.52****
Volatile Fine Particle Number	2.59×10^{14} $\overset{\times}{\div}$ 1.27	-	-	1.48×10^{14} $\overset{\times}{\div}$ 1.03	**0.57****
Non-Volatile Fine Particle Number	1.73×10^{14} $\overset{\times}{\div}$ 1.43	-	-	7.76×10^{13} $\overset{\times}{\div}$ 1.11	**0.45****
Total Particle Volume ($5 < D_p < 120$ nm) (mm^3)	9.46 $\overset{\times}{\div}$ 1.14	-	-	4.54 $\overset{\times}{\div}$ 1.46	**0.48***
Volatile Particle Volume (mm^3)	6.48 $\overset{\times}{\div}$ 1.00	-	-	1.19 $\overset{\times}{\div}$ 1.05	0.18
Non-Volatile Particle Volume (mm^3)	5.97 $\overset{\times}{\div}$ 1.39	-	-	2.33 $\overset{\times}{\div}$ 1.25	0.39
PSAP BC-Equivalent Mass at 467 nm (mg)	13.44 $\overset{\times}{\div}$ 1.02	-	-	4.21 $\overset{\times}{\div}$ 1.08	**0.31******
PSAP BC-Equivalent Mass at 530 nm (mg)	12.73 $\overset{\times}{\div}$ 1.03	-	-	4.06 $\overset{\times}{\div}$ 1.14	**0.32******
PSAP BC-Equivalent Mass at 660 nm (mg)	13.07 $\overset{\times}{\div}$ 1.09	-	-	4.08 $\overset{\times}{\div}$ 1.29	**0.31*****
Carbon Monoxide, CO (g)	8.14 ± 0.65	-	-	8.50 ± 1.72	1.04
Nitrogen Oxides, NO_x (g)	6.43 ± 0.36	-	-	6.19 ± 0.32	0.96
Number of Plume Intercepts	4	0		4	

Significance Level: **** $p < 0.001$, *** $p < 0.01$, ** $p < 0.05$, * $p < 0.1$

†Particle EIs are reported as the geometric mean $\overset{\times}{\div}$ the geometric standard deviation, while trace gas EIs are reported as the arithmetic mean $\pm$ the arithmetic standard deviation.

S4 References and Notes

1. C. Wey, *et al.*, Aircraft Particle Emissions eXperiment (APEX), *Tech. Rep. NASA/TM-2006-214382*, NASA (2006).

2. C. C. Wey, *et al.*, *Journal of Propulsion and Power* **23**, 898 (2007).

3. B. Anderson, *et al.*, Alternative aviation fuel experiment (AAFEX), *Tech. Rep. NASA/TM-2011-217059*, NASA (2011).

4. A. J. Beyersdorf, *et al.*, *Atmospheric Chemistry and Physics* **14**, 11 (2014).

5. R. H. Moore, *et al.*, *Energy & Fuels* **29**, 2591 (2015).

6. ASTM D2622: Standard test method for sulfur in petroleum products by wavelength dispersive x-ray fluorescence spectrometry, ASTM International. http://www.astm.org/Standards/D2622.htm.

7. ASTM D1319: Standard test method for hydrocarbon types in liquid petroleum products by fluorescent indicator absorption, ASTM International. http://www.astm.org/Standards/D1319.html.

8. ASTM D7171: Standard test method for hydrogen content of middle distililate petroleum products by low-resolution pulsed nuclear magnetic resonance spectroscopy, ASTM International. http://www.astm.org/Standards/D7171.htm.

9. ASTM D1840: Standard test method for naphthalene hydrocarbon in aviation turbine fuels by ultravultra spectrophotometry, ASTM International. http://www.astm.org/Standards/D1840.htm.

10. ASTM D4052: Standard test method for density, relative density, and API gravity of liquids by digital density meter, ASTM International. http://www.astm.org/Standards/D4052.htm.

11. ASTM D3338: Standard test method for estimation of net heat of combustion of aviation fuels, ASTM International. http://www.astm.org/Standards/D3338.htm.

12. ASTM D1655: Standard specificiation for aviation turbine fuels, ASTM International. http://www.astm.org/Standards/D1655.htm.

13. ASTM D7566: Standard specificiation for aviation turbine fuel containing synthesized hydrocarbons, ASTM International. http://www.astm.org/Standards/D7566.htm.

14. A. J. Beyersdorf, *et al.*, *Atmospheric Chemistry and Physics* **16**, 1003 (2016).

15. K. L. Thornhill, *et al.*, *Journal of Geophysical Research: Atmospheres* **113**, D08201 (2008).

16. B. E. Anderson, *et al.*, *Geophysical Research Letters* **25**, 1689 (1998).

17. R. H. Moore, *et al.*, *Aerosol Science and Technology* **48**, 467 (2014).

18. A. Virkkula, *Aerosol Science and Technology* **44**, 706 (2010).

19. T. C. Bond, R. W. Bergstrom, *Aerosol Science and Technology* **40**, 27 (2006).

20. S.-L. von der Weiden, F. Drewnick, S. Borrmann, *Atmospheric Measurement Techniques* **2**, 479 (2009).